Electron. Mater. Lett., Vol. 11, No. 1 (2015), pp. 46-54
DOI: 10.1007/s13391-014-4064-z

Structural, Morphological and Optical Properties of Sprayed Nanocrystalline Thin Films of $Cd_{1-x}Zn_xS$ Solid Solution

Urvashi Verma,* Vikas Thakur, Poolla Rajaram, and A. K. Shrivastava

School of Studies in Physics, Jiwaji University, Gwalior 474 011, India

(received date: 1 March 2014 / accepted date: 16 June 2014 / published date: 10 January 2015)

A series of nanocrystalline thin films of cadmium zinc sulphide ($Cd_{1-x}Zn_xS$) solid solution were deposited on glass substrates using spray pyrolysis. Cadmium chloride ($CdCl_2$), zinc chloride ($ZnCl_2$) and thiourea (NH_2CSNH_2) were used as the sources of Cd, Zn and S respectively. The films were characterized using structural, morphological and optical techniques. X-ray diffraction (XRD) studies show that the films of $Cd_{1-x}Zn_xS$ are polycrystalline and single phase having the wurtzite structure. The crystallites in the thin films of pure CdS possess preferred crystallographic orientation along the <002> direction. The preferred orientation of crystallites in the $Cd_{1-x}Zn_xS$ films changes from <002> to <101> with increase in Zn concentration. The lattice parameters of $Cd_{1-x}Zn_xS$ decrease with increase in Zn concentration. Scanning electron microscopy (SEM) and atomic force microscopy (AFM) studies show that the surfaces of the films are smooth and are uniformly covered with nanoparticles. Energy dispersive analysis of x-rays (EDAX) results reveal that the grown films have good stoichiometry. Optical transmission spectra confirm the good quality of the $Cd_{1-x}Zn_xS$ films.

Keywords: $Cd_{1-x}Zn_xS$, nanoparticles, XRD, SEM, AFM, UV-VIS spectroscopy

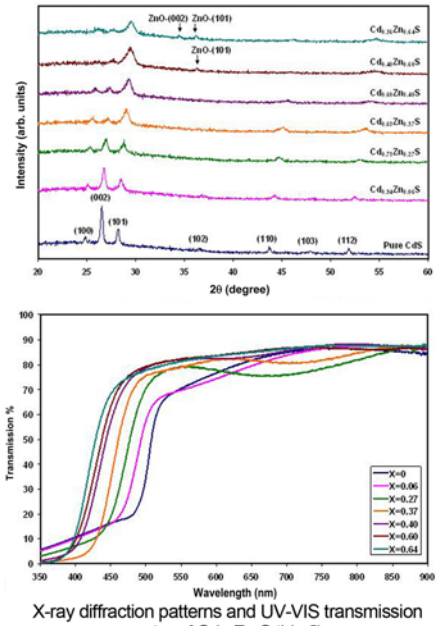

X-ray diffraction patterns and UV-VIS transmission spectra of $Cd_{1-x}Zn_xS$ thin films

1. INTRODUCTION

Cadmium Sulfide (CdS), a II-VI compound semiconductor having a wide band gap of 2.4 eV, has received a lot of attention among researchers, owing to its potential application in various opto-electronic devices.[1,2] CdS has received special focus on its application as a window layer in heterojunction solar cells. However, the heterojunction solar cells have low conversion efficiencies due to the fact that CdS is transparent only in a limited wavelength range. The use of Cadmium Zinc Sulfide $Cd_{1-x}Zn_xS$ as window layer instead of CdS, leads to a decrease in window absorption losses (due to its higher bandgap), thus increasing the efficiency of the heterojunction solar cells. $Cd_{1-x}Zn_xS$ semiconducting compounds are of great technological importance due to their tunable optical properties. The band gap of $Cd_{1-x}Zn_xS$ solid solution can be continuously adjusted from 2.4 eV (band gap of CdS) to 3.7 eV (band gap of ZnS) by changing its composition. The use of $Cd_{1-x}Zn_xS$ as a window layer in heterojunction solar cells having absorber layer of materials such as CdTe,[3,4] Cu_xS,[5,6] $CuInSe_2$,[7,8] and $CuGaSe_2$[9] have shown improved device performance and efficiency. Moreover, its tunable optical band gap allows $Cd_{1-x}Zn_xS$ to be used for short wavelength optoelectronic devices such as blue, violet, or even ultraviolet LED's, laser diodes and photodetectors.[10-12] Apart from optoelectronic applications, CdZnS also has potential applications in photo-electrochemical devices such as photoelectrochemical (PEC) cells (for solar energy conversion)[13] and photoelectrochemical/ photocatalytic cells for splitting of water for hydrogen production.[14-18] $Cd_{1-x}Zn_xS$ is preferred over CdS for photoelectrochemical/photocatalytic splitting of water because

*Corresponding author: u_verma@yahoo.com

the alloying of ZnS with CdS to form $Cd_{1-x}Zn_xS$ solid solution makes the conduction band edge more negative, resulting in a stronger driving force for water reduction.[19] The use of $Cd_{1-x}Zn_xS$ instead of CdS in PEC devices also has the advantage that it does not dissociate into its constituent ions in PEC conditions. CdS on the other hand, degrades into soluble cadmium cations, which are not only hazardous but also restrict the performance of the device.[13,20]

Several techniques have been employed to grow thin films of $Cd_{1-x}Zn_xS$ like vacuum evaporation,[21-24] electrochemical deposition,[25] successive ionic layer adsorption, reaction technique,[26] chemical vapor deposition,[27] chemical bath deposition (CBD),[13,28,29] spray pyrolysis,[30,31] etc. Spray pyrolysis is a very simple and inexpensive technique. It is basically a chemical deposition technique, in which a solution (aqueous/non-aqueous) containing salts of the desired elements are sprayed (with the help of a pressurized carrier gas) onto preheated substrates. Continuous films are formed on the substrates by the thermal decomposition of the reactants.

In this paper, we present our work on the growth and characterization of nanocrystalline thin films of $Cd_{1-x}Zn_xS$ - prepared using spray pyrolysis. The use of nanostructures in practical devices offers potential for better performance and higher efficiency, either by using new physical mechanisms appearing due to quantum confinement effects or by utilizing the increase in chemical activity due to availability of larger surface area. Similar work has also been reported by Baykul *et al.*.[30] However, our work differs from theirs in the sense that our material is nanocrystalline in nature. Furthermore, we have clearly shown in this work that there is an upper limit for Zn doping in CdS, above which other secondary phases like ZnO start growing.

2. EXPERIMENTAL PROCEDURE

$Cd_{1-x}Zn_xS$ films were deposited on glass substrates using spray pyrolysis. Cadmium chloride ($CdCl_2$), zinc chloride ($ZnCl_2$) and thiourea (NH_2CSNH_2) (all were of AR grade) were used as the starting materials. The aqueous solutions of $CdCl_2$ (0.1 M) and H_2NCSNH_2 (0.1 M) were mixed in the ratio of 1:2 and then a weighted amount of $ZnCl_2$ (as per requirement) was added to it. The amount of Cd in spray solution was kept constant while the amount of Zn was varied to obtain a series of $Cd_{1-x}Zn_xS$ films. A Cd:S ratio of 1:2 was taken in the spray solution to compensate for the loss of sulphur in the form of H_2S or SO_2 gas during deposition. The solution mixture was sprayed over the glass substrates which were kept on a hot iron plate heated to a temperature of 300°C. The films obtained were CdS, $Cd_{0.94}Zn_{0.06}S$, $Cd_{0.73}Zn_{0.27}S$, $Cd_{0.63}Zn_{0.37}S$, $Cd_{0.60}Zn_{0.40}S$, $Cd_{0.40}Zn_{0.60}S$ and $Cd_{0.36}Zn_{0.64}S$ (as determined from EDAX results).

In the spray pyrolysis process, the spray solution is forced through a fine nozzle converting the liquid into very fine droplets. When these droplets reach the hot substrate, they undergo pyrolytic decomposition resulting in the deposition of well adherent films. The particle size of materials grown using spray pyrolysis is known to depend on factors like nozzle size, spray rate and nature of spray solution e.g. colloidal or non-colloidal.[32] The smaller the size of the sprayed droplets, the smaller is the expected particle size of the resulting solid.[33] In our case, the size of the droplets was made very small using a spray nozzle of very fine pore (pore diameter was approximately 0.25 mm). The solution was sprayed onto the hot substrates at a rate of 2 mL/minute. A maximum of 2 mL of solution was sprayed at a time. The process of spray was repeated a few times in order to achieve the desired film thickness. A gap of 2 minutes was maintained between successive sprays in order to let any residual volatile impurity evaporate and also to ensure good crystallinity. The quality of the deposited films depends to a great extent on the cleaning of substrates. Well adherent and uniform films can only be deposited on highly clean surfaces. So, the process of rigorous cleaning of glass substrates using neutral detergent, chromic acid, acetone and ultrasonic treatment in de-ionized water was adopted to ensure a clean surface.

The films were characterized using x-ray diffraction (XRD), Scanning electron microscopy (SEM), Atomic force microscopy (AFM), energy dispersive x-ray spectroscopy (EDAX) and UV-VIS spectroscopy. XRD studies were carried out using an x-ray diffractometer (X'Pert-Pro) employing Cu K_α radiation of wavelength 1.5406 Å. Scanning electron microscopy (SEM) and energy dispersive x-ray spectroscopy (EDAX) studies were carried out using a Philips FE-SEM/EDAX-Quanta 200 FEG microscope. Atomic force microscopy (AFM) studies were performed on an NTMDT NTEGRA-model Surface Probe Microscope. Optical studies were carried out on a Shimadzu UV-2450 UV-VIS spectrophotometer.

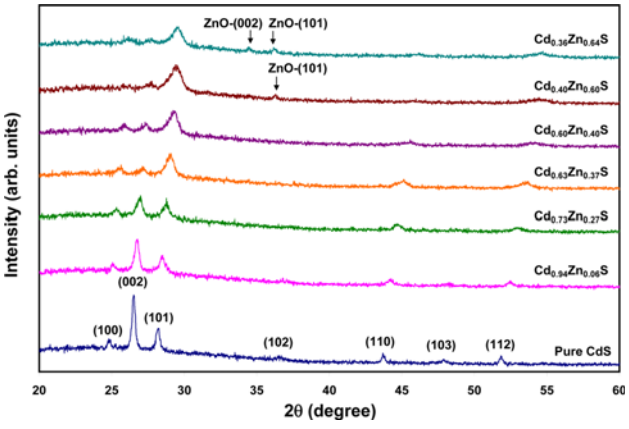

Fig. 1. X-ray diffraction patterns of $Cd_{1-x}Zn_xS$ films.

3. RESULTS AND DISCUSSION

3.1 Structural studies

Figure 1 shows the XRD patterns of $Cd_{1-x}Zn_xS$ thin films. It can be observed from XRD patterns that all the films are polycrystalline in nature. The broad diffraction peaks indicate the nanocrystalline nature of films.

For, x = 0.0 (i.e. pure CdS), the observed diffraction pattern and inter-planar spacings match with the standard diffraction pattern of CdS (JCPDS card number 41-1049), demonstrating the formation of wurtzite phase CdS. No phase other than the wurtzite CdS was detected in the XRD pattern. The crystallites in pure CdS were found to possess the preferred crystallographic orientation along <002> direction. XRD patterns of $Cd_{1-x}Zn_xS$ (for, x = 0.06, 0.27, 0.37, 0.40, 0.60 and 0.64) showed that these films too crystallized in the hexagonal wurtzite structure. The absence of any diffraction peak corresponding to the binary phase ZnS indicated that the films obtained were of $Cd_{1-x}Zn_xS$ solid solutions. It can also be observed from XRD patterns that the preferred orientation of the $Cd_{1-x}Zn_xS$ films shifts from <002> to <101> with the increase in Zn concentration.

The diffraction peaks of $Cd_{1-x}Zn_xS$ shifted to higher diffraction angles with the increase in Zn concentration. This indicates a decrease in the lattice parameters and hence the unit cell size of $Cd_{1-x}Zn_xS$ with the increase in Zn concentration. This is caused by the fact that the ionic radius of Zn (0.074 nm) is smaller than that of Cd (0.097 nm). When large-sized atoms in the lattice are replaced by smaller sized atoms, the whole lattice relaxes by decreasing its lattice parameters. The lattice parameters 'a' and 'c' for hexagonal phase $Cd_{1-x}Zn_xS$ have been calculated from the XRD data using the following equation,

$$\frac{1}{d^2} = \frac{4}{3}\left(\frac{h^2+hk+k^2}{a^2}\right) + \frac{l^2}{c^2} \quad (1)$$

Where, d is the interplanar spacing and (h, k, l) are the Miller indices of the plane. The values of the lattice parameters so calculated are listed in Table 1. The values of 'a' and 'c' for pure CdS match with standard values (JCPDS card number 41-1049) and were found to decrease with the addition of Zn as suggested above.

Table 1. Calculated values of lattice parameter, crystallite size and band gap energy of nanocrystalline thin films of $Cd_{1-x}Zn_xS$.

Sample	Lattice Parameters (Å)		Crystallite Size (Scherrer's Formula) (nm)	Band Gap (eV)
	a	c		
CdS (x = 0.0)	4.1395	6.7136	33.41	2.43
$Cd_{0.94}Zn_{0.06}S$	4.1041	6.6550	24.09	2.51
$Cd_{0.73}Zn_{0.27}S$	4.0554	6.6036	23.51	2.63
$Cd_{0.63}Zn_{0.37}S$	4.0044	6.5582	14.24	2.79
$Cd_{0.60}Zn_{0.40}S$	3.9763	6.5254	13.09	2.92
$Cd_{0.40}Zn_{0.60}S$	3.9660	6.4186	09.31	3.08
$Cd_{0.36}Zn_{0.64}S$	3.9326	6.4156	13.10	3.12

No peaks other than wurtzite $Cd_{1-x}Zn_xS$ were observed for $x \leq 0.40$ but for $x \geq 0.60$, weak intensity extraneous peaks were present at diffraction angles (2θ) equal to 34.4 and 36.2 degrees. These extraneous peaks were found to belong to the hexagonal phase of ZnO (JCPDS, 36-1,451). The growth of a small amount of ZnO along with CdZnS is probably due to the oxidation of excess Zinc to form ZnO as secondary phase. The formation of ZnO as secondary phase may be avoided by replacing the carrier gas oxygen with nitrogen.

The average crystallite size was calculated using the well known XRD line broadening method (Scherrer's equation),

$$D = \frac{0.9\lambda}{B\cos\theta} \quad (2)$$

where, D is the average crystal size, λ is the wavelength of x-rays, B is the full width at half maximum and θ is the diffraction angle. The calculated crystallite sizes are in the nanometer range and have been given in Table 1. The crystallite size is found to decreases with the increase in Zn concentration in $Cd_{1-x}Zn_xS$.

3.2 Surface morphology

The surface morphology of the $Cd_{1-x}Zn_xS$ thin films has been studied using SEM and AFM. Figures 2(a), (b), (c), (d), (e), (f) and (g) show the SEM micrographs of $Cd_{1-x}Zn_xS$ films for x = 0.0, 0.06, 0.27, 0.37, 0.40, 0.60 and 0.64 respectively. It can be clearly observed from SEM images that the surfaces of all films are uniformly covered with nanoparticles and that the particle size decreases slightly with the increase in Zn concentration. The SEM images showed that the $Cd_{1-x}Zn_xS$ films (for x = 0.0, 0.06, 0.27, 0.37, 0.40) have smooth surfaces with uniform morphology all over the surface. However, for $Cd_{0.40}Zn_{0.60}S$ and $Cd_{0.36}Zn_{0.64}S$ films, there is a peculiar growth at some spots. This peculiar growth may be due to the formation of oxide species (ZnO) at these spots (also predicted in XRD studies). Figures 3(a), (b), (c), (d), (e), (f) and (g) show the 2D and 3D AFM micrographs of $Cd_{1-x}Zn_xS$ films for x = 0.0, 0.06, 0.27, 0.37, 0.40, 0.60 and 0.64 respectively. The AFM studies again clearly show that the surfaces of the films are uniformly covered with nanoparticles. The size of the nanoparticles measured from SEM and AFM micrographs is around 40 to 50 nm, which is slightly larger than the sizes measured from XRD. This may be due to the fact that the particles viewed in SEM and AFM micrographs are probably agglomerated nanocrystals. The peculiar growth spots can be clearly viewed in 3D AFM images of $Cd_{1-x}Zn_xS$ films having higher Zn concentration. The average surface roughness for $Cd_{1-x}Zn_xS$ films for x = 0.0, 0.06, 0.27, 0.37, 0.40, 0.60 and 0.64 is of the order of 10, 6, 7, 8, 9, 23 and 30 nm

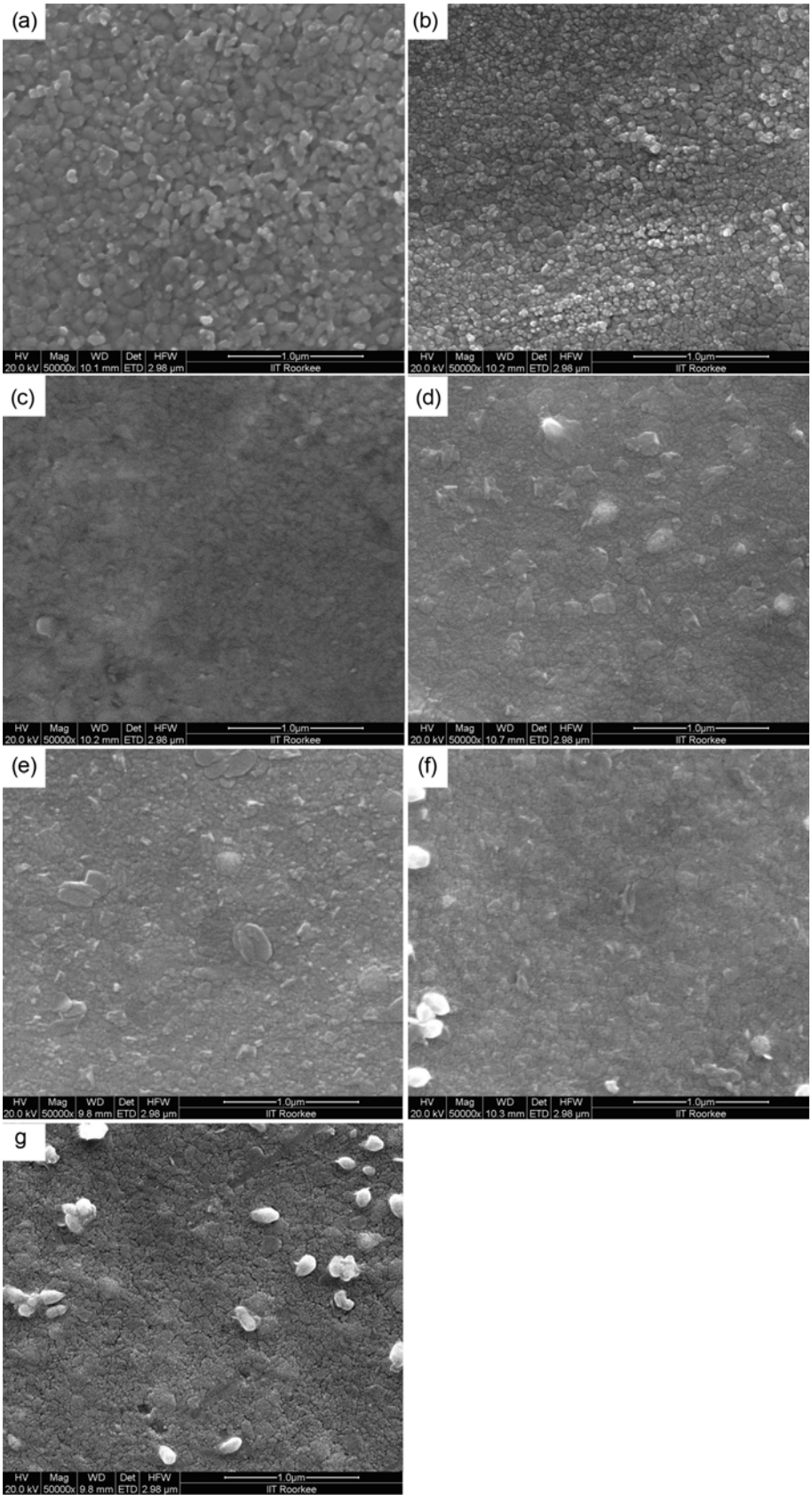

Fig. 2. SEM micrographs of $Cd_{1-x}Zn_xS$ thin films (a) $x = 0.00$ (b) $x = 0.06$, (c) $x = 0.27$, (d) $x = 0.37$, (e) $x = 0.40$, (f) $x = 0.60$ and (g) $x = 0.64$.

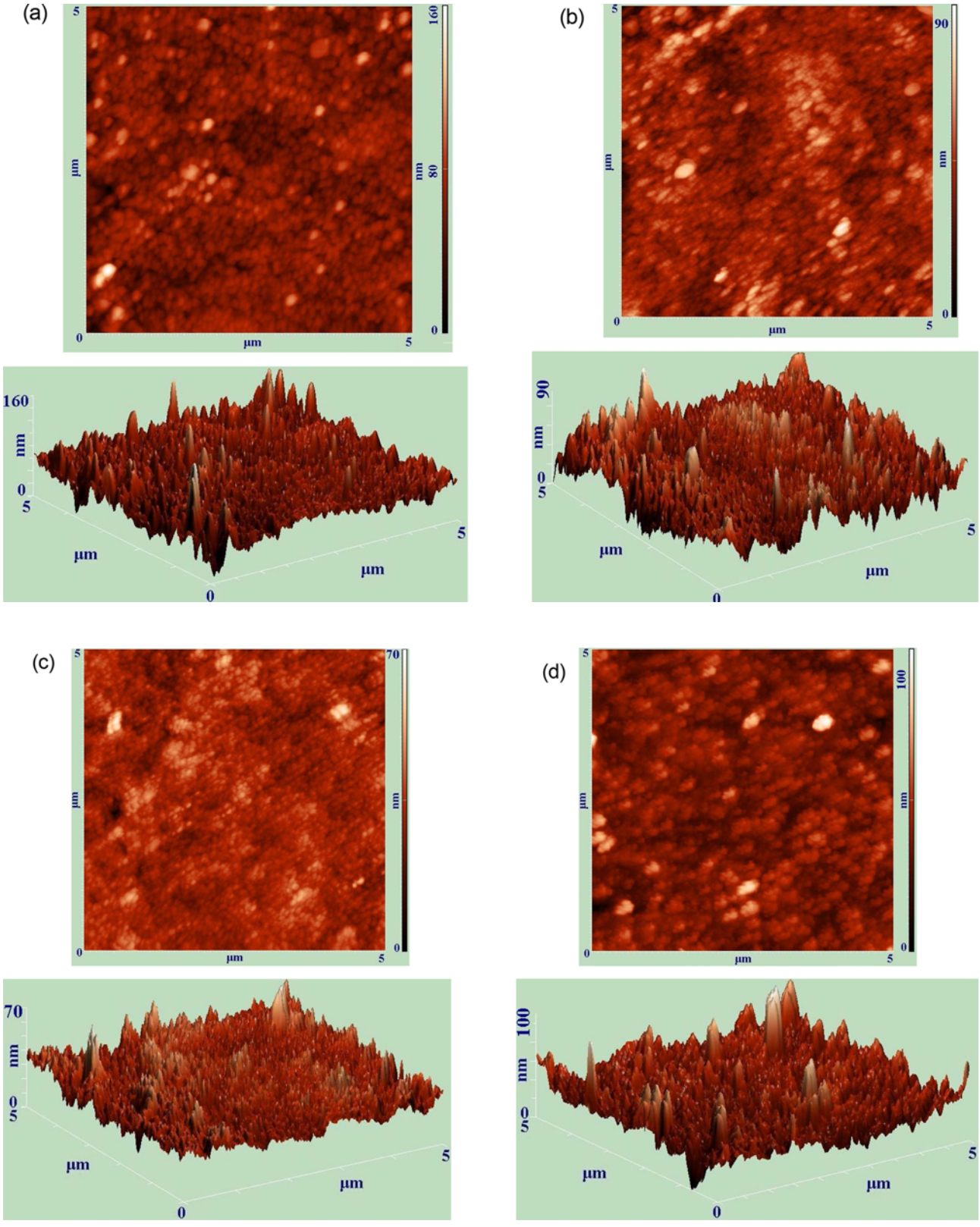

Fig. 3. (a) 2D & 3D AFM micrographs of CdS Thin Film, (b) 2D & 3D AFM micrographs of $Cd_{0.94}Zn_{0.06}S$ Thin Film, (c) 2D & 3D AFM micrographs of $Cd_{0.73}Zn_{0.27}S$ Thin Film, (d) 2D & 3D AFM micrographs of $Cd_{0.63}Zn_{0.37}S$ Thin Film, (e) 2D & 3D AFM micrographs of $Cd_{0.60}Zn_{0.40}S$ Thin Film, (f) 2D & 3D AFM micrographs of $Cd_{0.40}Zn_{0.60}S$ Thin Film, (g) 2D & 3D AFM micrographs of $Cd_{0.36}Zn_{0.64}S$ Thin Film.

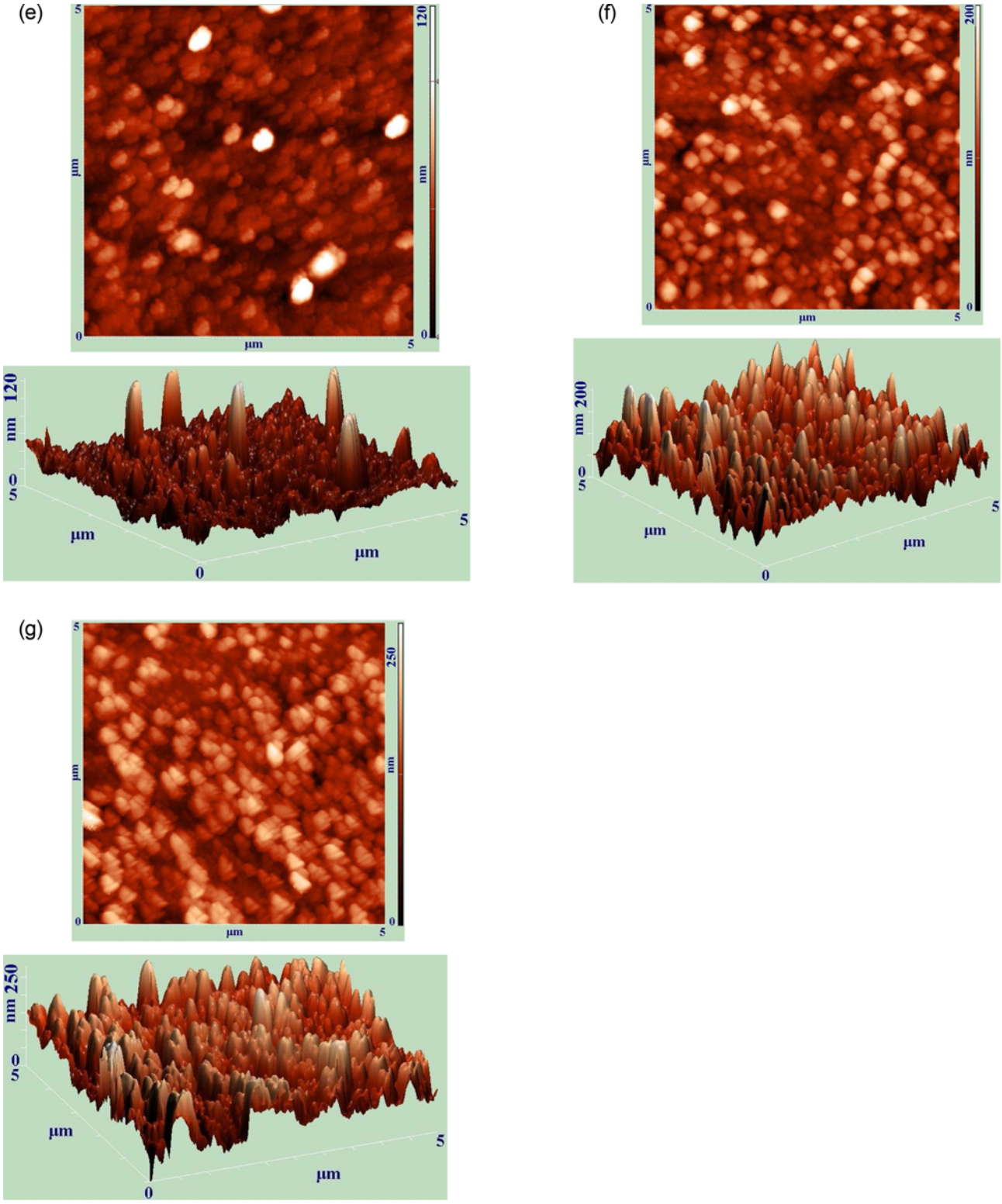

Fig. 3. Continued.

respectively, which confirms the highly smooth surface of films. The roughness of the film for $x = 0.60$ and 0.64 is slightly larger than for films of other compositions.

3.3 Elemental composition

The elemental composition of $Cd_{1-x}Zn_xS$ films was obtained by EDAX. Table 2 shows the composition of elements in the

Table 2. Elemental compositions in initial spray solution and $Cd_{1-x}Zn_xS$ solid solution.

Sample ($Cd_{1-x}Zn_xS$)	Atomic percentage in initial spray solution			Atomic percentage in grown $Cd_{1-x}Zn_xS$ solid solution (EDAX analysis)		
	Cd	Zn	S	Cd	Zn	S
CdS (x = 0.0)	50.00	0.00	50.00	47.96	0.00	52.04
$Cd_{0.94}Zn_{0.06}S$	47.50	2.50	50.00	45.78	3.09	51.13
$Cd_{0.73}Zn_{0.27}S$	45.00	5.00	50.00	39.84	14.87	45.29
$Cd_{0.63}Zn_{0.37}S$	40.00	10.00	50.00	34.80	20.39	44.81
$Cd_{0.60}Zn_{0.40}S$	35.00	15.00	50.00	30.24	20.20	49.56
$Cd_{0.40}Zn_{0.60}S$	30.00	20.00	50.00	21.38	32.53	46.10
$Cd_{0.36}Zn_{0.64}S$	25.00	25.00	50.00	19.99	35.12	44.89

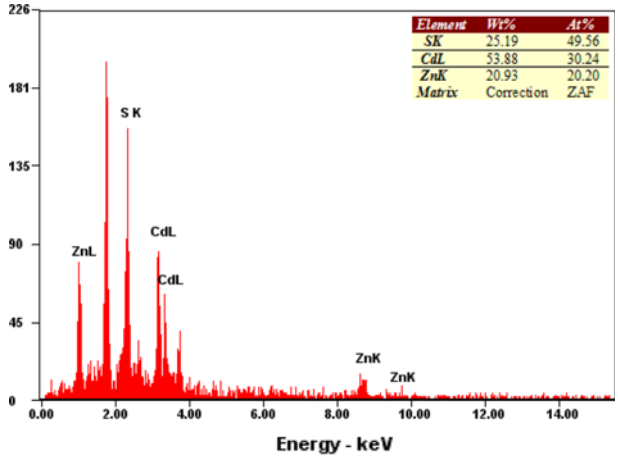

Fig. 4. EDAX spectrum of $Cd_{0.60}Zn_{0.40}S$ thin film.

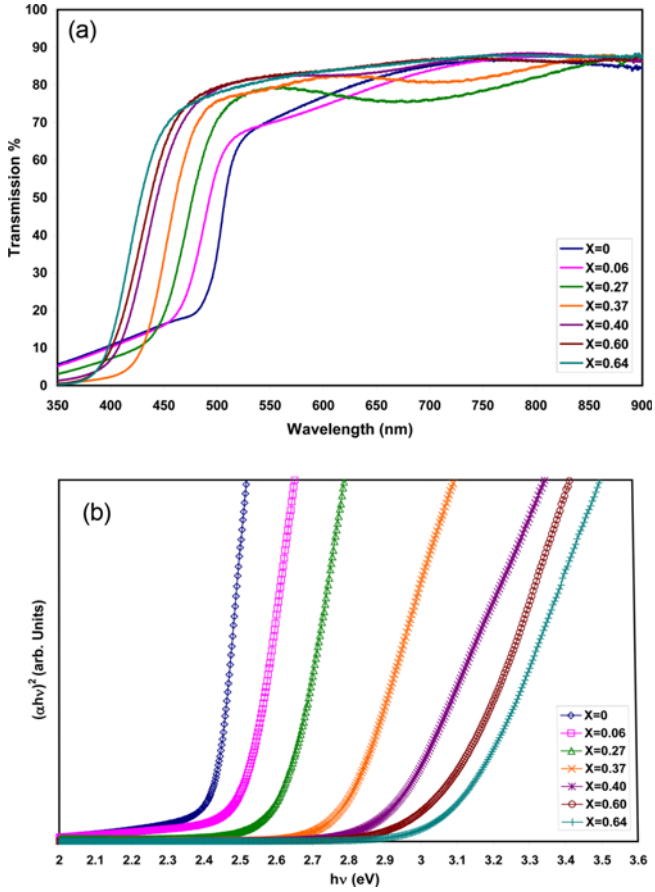

Fig. 5. (a) UV-VIS transmission spectra of $Cd_{1-x}Zn_xS$ thin films, (b) $(\alpha h\nu)^2$ versus hν plot of $Cd_{1-x}Zn_xS$ thin films.

sprayed solution (determined from the amount of Cd, Zn and S salts used to prepare the spray solution) and composition of elements in grown films (determined using EDAX). EDAX studies confirmed the presence of Cd, Zn and S in grown films. EDAX results revealed that the grown films have good stoichiometry i.e. Cd (atom %) + Zn (atom %) ≈ S (atom %) = 50%. The quantity of S has been found to be slightly less in some films which may be due to evaporation of S in the form H_2S or SO_2 gas during the growth. The amount of thiourea can be slightly increased in the initial spray solution to increase S in the films. It can also be observed from Table 2 (by comparing Zn composition in initial spray solutions and in films), that Zn assimilates into the $Cd_{1-x}Zn_xS$ solid solution slightly in excess as compared to Cd. These results show that Zn has large solubility in CdS lattice. The EDAX spectrum with elemental composition for one of the samples ($Cd_{0.60}Zn_{0.40}S$) is shown in Fig. 4.

3.4 Optical properties

Figure 5(a) shows the UV-VIS transmission spectra of the $Cd_{1-x}Zn_xS$ thin films. The films exhibit very high optical transmission in the visible range (below the absorption edge), which is important for their applications as window layers in hetrojunction solar cells. The sharp absorption corresponding to the band edge confirms the good quality of grown films. A blue shift occurs in the absorption edge of $Cd_{1-x}Zn_xS$ films with the increase in Zn concentration, which indicates that the band gap of $Cd_{1-x}Zn_xS$ increases with increase in Zn concentration. The optical band gap of the samples was determined by the following Tauc relationship,[34]

$$(\alpha h\nu) = A(h\nu - E_g)^m \quad (3)$$

Figure 5(b) shows the plot of $(\alpha h\nu)^2$ against photon energy $h\nu$ and the values of direct optical gaps were determined by the straight line intercepts on the $h\nu$ axis. The values of the optical band gap energies for the $Cd_{1-x}Zn_xS$ films for $x = 0.0$, 0.06, 0.27, 0.37, 0.40, 0.60 and 0.64 were found to be 2.43, 2.51, 2.63, 2.79, 2.92, 3.08 and 3.12 eV respectively. It is clear that the band gap increases with the increase in Zn concentration in $Cd_{1-x}Zn_xS$. This shows that the band gap of $Cd_{1-x}Zn_xS$ can be tailored by simply varying the Cd:Zn ratio. This controlled band gap alignment is useful in fabrication of short wavelength LEDs, Laser diodes, short wavelength photo-detectors, photo-electrode material for PEC cells and photocatalytic material for splitting of water for hydrogen production.

This increase in band gap is purely due to the alloying of higher band gap ZnS with lower band gap CdS compounds to form CdZnS solid solution and cannot be regarded as a quantum confinement effect. The quantum confinement effect causes a blue shift in absorption edge corresponding to the band gap of nanoparticles. The quantum confinement effect in nanoparticles should be observable when the particle size reduces to the scale of an exciton Bohr radius. CdS has a small exciton Bohr radius of the order of 2.8 nm. The particles grown in our cases are larger than the exciton Bohr radius of CdS or CdZnS due to which the quantum confinement effect is not expected. In spite of this, however, these nanoparticles are expected to show enhanced chemical activity due to the availability of larger surface area (owing to increase in the surface to volume ratio) compared to the bulk material and may be beneficial in PEC cell and photocatalytic material for splitting of water for hydrogen production.

4. CONCLUSIONS

Nanocrystalline thin films of $Cd_{1-x}Zn_xS$ were grown using spray pyrolysis. A sprayer having a nozzle of very fine pore (pore size 0.25 mm) generated a mist of very small droplets from the spray solution. On reaching the hot substrates, these droplets thermally decomposed to form uniformly distributed CdZnS nanoparticles. XRD studies show that the films of $Cd_{1-x}Zn_xS$ are polycrystalline and single phase having the wurtzite structure. The lattice constants of $Cd_{1-x}Zn_xS$ decrease with the increase in Zn concentration. At high Zn concentrations in the initial spray solution, ZnO was found to grow as a secondary phase along with CdZnS. SEM and AFM studies show that the smooth surfaces of the films contain nanoparticles of sizes around 40 - 50 nm. The particle size is found to decrease with the increase in Zn concentration in $Cd_{1-x}Zn_xS$. EDAX studies confirm the presence of Cd, Zn and S close to the required composition. UV-VIS studies confirm that the films have very high optical transmission in the visible region. The band gap of $Cd_{1-x}Zn_xS$ can be continuously modulated (decreased or increased) by adjusting the Cd:Zn ratio. The use of these nanocrystalline $Cd_{1-x}Zn_xS$ films in PEC cell and photocatalytic material for splitting of water for hydrogen production is expected to result in enhanced performance and efficiency of these devices due to an increase in the active surface area.

ACKNOWLEDGMENTS

The authors are grateful to Prof. Ramesh Chandra, Mr. Shiv kumar, Mr. S.D.Sharma and Mr. B. Dutt, IIC, Indian Institute of Technology (IIT) Roorkee for providing the XRD, SEM and AFM facilities.

REFERENCES

1. M. Ichimura, F. Goto, and E. Arai, *J. Appl. Phys*. **85**, 7411 (1999).
2. X. Xu, J. CesaranoIII, E. Burch, and G. P. Lopez, *Thin Solid Films* **305**, 95 (1997).
3. O. M. Hussain, P. S. Reddy, B. S. Naidu, U. Uthanna, and P. J. Reddy, *Semicond. Sci. Technol.* **6**, 690 (1991).
4. T. L. Chu, S. S. Chu, J. Britt, C. Feredikes, and C. Q. Wu, *J. Appl. Phys.* **70**, 2688 (1991).
5. L. C. Burton and T. L. Hetch, *Appl. Phys. Lett.* **29**, 612 (1976).
6. H. L. Kwok, *J. Phys. D: Appl. Phys.* **16**, 2367 (1983).
7. R. R. Potter and J. R. Sites, *Appl. Phys. Lett.* **43**, 843 (1983).
8. J. W. Bowron, S. D. Damaskinos, and A. E. Dixon, *Sol. cells* **31**, 159 (1991).
9. K. T. R. Reddy and P. J. Reddy, *J. Phys. D: Appl. Phys.* **25**, 1345 (1992).
10. B. J. Wu, H. Cheng, S. Guha, M. A. Haase, J. M. De Puydt, G. Meis-Haugen, and J. Qiu, *Appl. Phys. Lett.* **63**, 2935 (1993).
11. J. H. Lee, W. C. Song, K. J. Yang, and Y. S. Yoo, *Thin Solid Films* **416**, 184 (2002).
12. M. A. Redwan, L. I. Soliman, E. H. Aly, A. A. El-Shazely, and H. A. Zayed, *J. Mater. Sci.* **38**, 3449 (2003).
13. P. B. Bagdare, S. B. Patil, and A. K. Singh, *J. Alloys Compd.* **506**, 120 (2010).
14. M. Li, J. Jiang, and L. Guo, *Int. J. Hydrogen Energy* **35**, 7036 (2010).
15. A. Kudo and Y. Miseki, *Chem. Soc. Rev.* **38**, 253 (2009).
16. F. E. Osterloh, *Chem. Mater.* **20**, 35 (2008).
17. K. Maeda, K. Teramura, D. L. Lu, T. Takata, N. Saito, and Y. Inoue, *Nature* **440**, 295 (2006).
18. D. Jing, Y. Zhang, and L. Guo, *Chem. Phys. Lett.* **415**, 74 (2005).
19. X. Zhang, D. Jing, M. Liu, and L. Guo, *Catal. Commun.* **9**, 1720 (2008).

20. A. H. Zyoud, N. Zaatar, I. Saadeddin, C. Ali, D. Park, G. Campet, and H. S. Hilal, *J. Hazard. Mater*. **173**, 318 (2010).
21. R. Menner, B. Dimmler, R. H. Mauch, and H. W. Schock, *J. Cryst Growth* **86**, 906 (1988).
22. D. Patidar, N. S. Saxena, and T. P. Sharma, *J. Modern Optics* **55**, 79 (2008).
23. P. Kumar, A. Misra, D. Kumar, N. Dhama, T. P. Sharma, and P. N. Dixit, *Optical Mater.* **27**, 261 (2004).
24. J. Torres and G. Gordillo, *Thin Solid Films* **310**, 310 (1997).
25. F. Loglio, M. Innocenti, G. Pezzatini, and M. L. Foresti, *J. Electroanal. Chem.* **562**, 117 (2004).
26. G. Laukaitis, S. Lindroos, S. Tamulevicius, M. Leskela, and M. Rackaitis, *Appl. Surf. Sci.* **161**, 396 (2000).
27. M. Nyman, K. Jenkins, M. J. H. Smith, T. T. Kodas, E. N. Duester, A. L. Rheingold, and M. L. L. Sands, *Chem. Mater.* **10**, 914 (1998).
28. S. Chavhan and R. P. Sharma, *J. Phys. Chem. Solids* **66**, 1721 (2005).
29. S. D. Chavhan, S. Senthilarasu, and S. H. Lee, *Appl. Surf. Sci.* **254**, 4539 (2008).
30. M. C. Baykul and N. Orhan, *Thin Solid Films* **518**, 1925 (2010).
31. Y. Raviprakash, K. V. Bangera, and G. K. Shivakumar, *Sol. Energy* **83**, 1645 (2009).
32. A. K. Sharma and P. Rajaram, *Mater. Sci. Eng. B* **172**, 37 (2010).
33. K. Okuyama and I. W. Lenggoro, *Chem. Eng. Sci.* **58**, 537 (2003).
34. J. Tauc, *Amorphous and Liquid Semiconductors,* Plenum Press, New York (1974).